Available online at www.sciencedirect.com
ScienceDirect
Journal of the European Ceramic Society 29 (2009) 1713–1720
www.elsevier.com/locate/jeurceramsoc

Bipolar strain hysteresis of poled composites with Nd–Mn-doped PZT fibres

C. Pientschke [a,*], A. Kuvatov [a], R. Steinhausen [a], H. Beige [a], R. Krüger [b], T. Müller [b], U. Helbig [b], D. Sporn [b], C. Schuh [c], S. Denneler [c], T. Richter [d], H. Schlich [e]

[a] *Martin-Luther-University Halle-Wittenberg, Physics Department, PFM, 06099 Halle, Germany*
[b] *Fraunhofer ISC, Neunerplatz 2, 97082 Würzburg, Germany*
[c] *Siemens AG, Corporate Technology, Ceramics, CT MM 2, Otto-Hahn-Ring 6, 81739 Munich, Germany*
[d] *VDO Automotive AG, Continental Group, 93055 Regensburg, Germany*
[e] *MaTeck GmbH, Im Langenbroich 20, 52428 Jülich, Germany*

Received 4 July 2008; received in revised form 18 September 2008; accepted 29 September 2008
Available online 10 December 2008

Abstract

Nd–Mn-doped PZT fibres were produced using the sol–gel process. The PZT was doped with 2 mol% neodymium and an amount of 1.1 mol% or 0.75 mol% manganese. The fibres were investigated with respect to microstructure, composition after sintering and phase content. Strain and polarisation were measured after imbedding the fibres in a polymer matrix.

The resulting 1–3-composites were poled with constant electric field. Measurements of strain and polarisation were done using a sinusoidal voltage of high amplitude. Instead of a shifted strain hysteresis (butterfly loop) an asymmetric strain–field relation was observed. The asymmetry depends on the direction of the applied voltage. For the half wave with voltage parallel to former poling voltage the strain curve is linear. For the other half wave the strain curve inflates and there is a region with no change of strain. Possible explanations for the asymmetric strain behaviour are discussed.

PACS: 77.84.Dy; 77.65.−j

Keywords: A. Sol–gel processes; B. Composites; C. Ferroelectric properties; C. Piezoelectric properties; D. PZT

1. Introduction

Piezoceramics based on the solid solutions of lead zirconate titanate (PZT) found a wide variety of technological application for decades.[1] PZT is tunable over a wide range of dielectric and electromechanical properties by varying the chemical composition.[2]

In this paper PZT fibres are presented that show in poled state a significant asymmetry in the piezoelectric strain. The production of fibres via sol–gel-route causes small grain sizes (about 1 μm) compared with bulk PZT fabricated by powder techniques. The diameter of the fibres is smaller than 60 μm. Therefore, the macroscopic properties were determined on 1–3-composites with embedded fibres. In contrast to several previous experiments given in the literature (for instance Refs. [3,4]) the samples were poled for a long time with a constant electric field strength and afterwards the samples were characterised with bipolar voltages. The special shape of strain loops is supposed to solely originate from the properties of the ceramic fibres.

2. Experimental procedure

2.1. Sol synthesis

Spinnable sols of the composition

$$Pb_{0.98}Nd_{0.02}([Zr_{0.545},\ Ti_{0.455}]_{1-x}Mn_x)O_3,\ x{=}0.011 \text{ or } 0.0075$$

were prepared by the following procedure: for 1 mol doped PZT the appropriate amounts of titanium ethoxide and zirconium propoxide were carboxylated by dissolving in 0.5 mol

* Corresponding author. Tel.: +49 345 55 25549; fax: +49 345 55 27158.
E-mail address: christoph.pientschke@physik.uni-halle.de (C. Pientschke).

0955-2219/$ – see front matter © 2008 Elsevier Ltd. All rights reserved.
doi:10.1016/j.jeurceramsoc.2008.09.026

caprylic acid. After 10 min of stirring 3.5 mol propionic acid were added and the solution was again stirred for further 30 min. 1.02 mol lead oxide, manganese acetate and neodymium acetate (0.02 mol) were added and went into solution during refluxing the liquid for 3 h at 120 °C. Finally excess solvent was removed by rotational evaporation at 120 °C at a pressure that was reduced by degrees down to 30 mbar. After cooling to room temperature a solid mass was obtained and crushed into granulate.

2.2. Fibre spinning, pyrolysing and sintering

The sol was heated to about 150 °C in a pressure vessel and continuously spun to fibres that were wound on a bobbin in several layers. Fibres with the length of one perimeter (50 cm) were cut from the bobbin and dried for 2 days each at 30, 50 and 110 °C to stabilise the fibres.

These fibres were pyrolysed as follows. Using an in-house built furnace the fibres were heated first to 250 °C (5 h holding time, steam atmosphere). Second, during a ramp (3.9 K/min) up to 700 °C the furnace was purged with air. Then the fibres cooled down following the furnace characteristics. After this process the fibres were in their oxide composition. The microstructure was very fine grained (<0.5 μm), porous and the only phase detectable by XRD was perovskite.

Sintering of the fibres was done on zirconia-coated alumina sheets in alumina containers that were closed by a lid. The PbO partial pressure inside the container was controlled during sintering by the addition of atmospheric powder (a 90/10 mixture of $PbZrO_2$ and PbO). This was done to prevent perovskite decomposition by PbO depletion of the fibres. With a heating rate of 5 K/min the furnace was heated to 900 °C (batches 1–3). To obtain very coarse grained fibres batch 4 was fired at 1200 °C. The isothermal sintering temperature was dwelled for 2 h. Then the heating was switched off and the samples cooled inside the furnace.

2.3. Fabrication of 1–3-composites

Composites with a 1–3 arrangement of PZT fibres in epoxy resin L160 and hardener L163 (MGS Kunstharzprodukte GmbH, Stuttgart, Germany) were prepared to characterise the electromechanical properties of the fibres. A bundle of approximately 40 mm long, parallel fibres was vacuum infiltrated by epoxy resin. The incorporation of gas bubbles was avoided by vacuum degassing of the resin prior to infiltration. The infiltrated bundle was compressed to increase its fibre content. Then the resin was cured for 24 h at room temperature. For better handling, the composite rod with a diameter of approximately 5 mm was molded into a 15 mm × 15 mm block of the same epoxy resin and cured for 24 h at 100 °C. Perpendicular to the fibre direction slices were cut with a wire saw and ground to a thickness of 0.5 mm. The fibre volume content was measured from SEM images. Gold electrodes were sputtered with Sputtering system (Type MED 010, Balzers, Liechtenstein) on both surfaces.

Composition, sintering temperature and fibre content of the batches can be found in Table 1.

Table 1
Composition and properties of the fibres. The batches are ordered with respect to rising grain size.

Properties	Batch			
	1	2	3	4
Mn-doping x (mol%)	1.1	1.1	0.75	1.1
Sintering at (°C)	900	900	900	1200
Fibre content (%)	53.7	46.0	42.7	34.3
Fibre diameter (μm)	54.3 ± 4.2	45.0 ± 8.2	39.5 ± 11.9	25.1 ± 6.2
Grain size (μm)	0.84 ± 0.39	0.98 ± 0.47	1.36 ± 0.70	15.5 ± 7.0
Grain size/fibre diameter (%)	1.5	2.2	3.4	61.8

3. Characterisation

Fibre composition of samples from batches 1 and 4 was investigated by microprobe analysis (JEOL JXA 8900 Superprobe) at the Institute for Mineralogy, University of Münster. Fibre samples were prepared by embedding into epoxy resin and polishing. At 10 points, the compositions were measured and averaged. Quantification of the experimental data was done without comparative measurements on a PZT standard.

SEM images were taken (Model S800, Hitachi Co. Ltd., Tokyo, Japan) of the bare sintered fibres to characterise the grain size (distribution) and of the composite slices to analyse the fibre content within the resin. Grain sizes (Feret diameters) were determined from top view images of the fibre surface. Maximum grain dimensions were measured in the direction of the fibre axis.

Phase analysis was done by X-ray diffraction of pulverised fibres (D5005, Bruker AXS/Siemens, Karlsruhe, Germany). Rietveld refinement of the data was performed with the software TOPAS3 (Bruker AXS). Lanthanum hexaboride (LaB6, NIST 660a) was used as an external standard. Scaling factors and lattice parameters were refined simultaneously. The dopant ions and the results of chemical analysis were incorporated into the structure data. Several models were tested: the samples were assumed to be single phase cubic, single phase rhombohedral and phase mixtures between cubic–tetragonal and rhombohedral–tetragonal.

The composite samples were poled in silicone oil with an applied electric field of 7.11 kV/mm. For generating high voltages the amplifier TREK 609D-6 (Trek Inc., Medina, NY, USA) was used. During the first 30 min the samples were tempered at 80 °C and for the following 60 min the field was maintained while the oil-bath cooled down to nearly room temperature. After relaxation of at least 12 h the samples were characterised at room temperature.

The hysteresis of strain and polarisation of the samples were measured with a sinusoidal voltage with frequency 10 Hz. The strain S_3 of the composites in poling direction was measured with a capacitive displacement sensor. Each measurement was calibrated with a certain displacement of a quartz crystal. The measuring setup is described in detail in Ref. [5].

Table 2
Fibre composition according to synthesis and microprobe analysis. Results are normalised to a total of B-site cations of 1. After batch number the sintering temperature is noted.

Batch	A-site cations		B-site cations			(Pb + Nd)/(Zr + Ti + Mn)
	Pb	Nd	Zr	Ti	Mn	
Synthesis	0.980	0.020	0.539	0.450	0.011	1
1 (900 °C)	0.964 ± 0.014	0.013 ± 0.002	0.563 ± 0.015	0.423 ± 0.010	0.014 ± 0.003	0.977
4 (1200 °C)	0.944 ± 0.015	0.013 ± 0.002	0.583 ± 0.017	0.409 ± 0.020	0.008 ± 0.002	0.957

The dielectric polarisation was measured by a modified Sawyer-Towers-circuit. Therefore, in poled samples solely differences of polarisation due to remanent polarisation were measured. The origin of such graphs is then chosen, either as zero or in a way that forces symmetry of maximum and minimum polarisation. The values of polarisation represent the properties of the fibres having regard to the fibre content but neglecting the mechanical clamping by the polymer. The given strain stands for the strain of the composite. A rough estimation following Ref. [6] shows that neglecting the mechanical clamping minimises the polarisation by less than 5%. Accordingly, the deviation between the composite and the fibre strains is smaller than 7% for all samples.

4. Results

4.1. Microprobe analysis

The fibre composition obtained from microprobe analysis of samples sintered at 900 °C and 1200 °C is given in Table 2 together with the composition from initial weights of the synthesis. Since no standard material was available, deviations exist between microprobe results and the composition according to initial weights from synthesis procedure.

Following we address the compositional differences determined between samples 1 and 4 which were determined by the same method (microprobe analysis). Compared to the sample 1 that was sintered at 900 °C, the 1200 °C sample 4 shows a slight depletion of lead, manganese and titanium and a gain of zirconium compared to the 900 °C sample.

The volatility of PbO is a well-known phenomenon.[7] Obviously the $PbZrO_3$/PbO buffer did not fully compensate the loss of PbO though having a higher partial pressure than PZT/PbO.[7] At 1229 °C MnO has a vapour pressure of 1.33×10^{-4} mbar.[8] The assumption of manganese oxide evaporation from the doped PZT fibres gets further support by the observation that

(1) the dark brown-grey colour of the pyrolysed and 900 °C sintered samples had faded for the 1200 °C sample and
(2) the ceramic supports of the fibres became brown in the vicinity of the fibres.

The vapour pressures of TiO_2 and TiO are about 3 and 1–2 orders of magnitude lower than the one of MnO, respectively.[8]

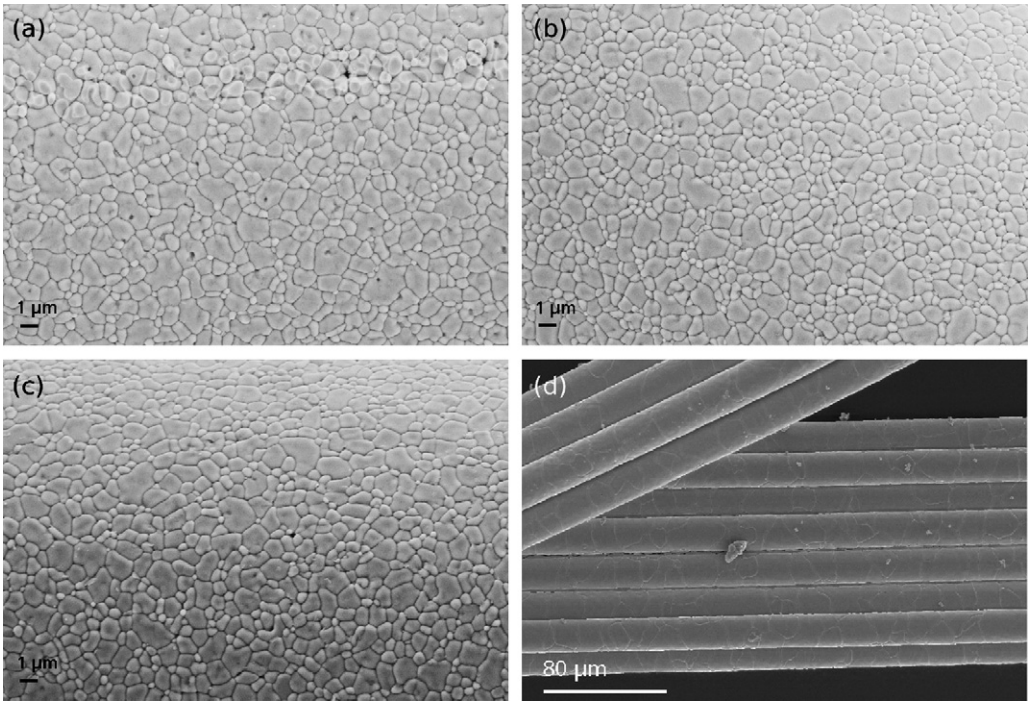

Fig. 1. Microstructure of the fibres from (a) batch 1 (1.1 mol% Mn, sintering at 900 °C), (b) batch 2 (see batch 1), (c) batch 3 (0.75 mol% Mn, sintering at 900 °C), and (d) batch 4 (1.1 mol%, sintering at 1200 °C).

Formation and evaporation of the suboxide TiO during sintering in air should happen only to a minor extent. Zirconia has an even lower vapour pressure so that it appears unreasonable to assume vapour transport of zirconia. The increase in zirconium content of the fibres is believed to result from the depletion of other cations since the cation content was normalised to 1.

4.2. Microstructure

After sintering the pyrolysed fibres SEM investigations of fibres were done. At the fibre surface the individual grains are visible (Fig. 1a–d). The fibres sintered at 900 °C exhibit a fine grained polycrystalline microstructure.

The mean grain sizes are given in Table 1. For all samples the distribution of the individual grain sizes appeared log-normal (data not shown). The grains of the fibres sintered at 900 °C were all below 3 μm, the smallest ones being those of sample 1. Compared to this, grains of sample 2 are only very slightly enlarged, those of sample 3 a bit more. The small difference between samples 1 and 2 are regarded to stem from small variance in the fibre arrangement during sintering. The grains of sample 3 presumably grew larger because of the smaller amount of Mn doping. For sample 4 grain sizes are considerably larger. The bigger grains exceed the fibre diameter. This drastic grain growth clearly comes from the high sintering temperature of 1200 °C and presumably from the loss of Mn.

4.3. Phase composition

Considering the *R*-values (agreement parameters of Rietveld refinement, further details see Table 3), best results were obtained with the two-phase model rhombohedral–tetragonal. As an example, the refinement results for sample 1 are given in Fig. 2. All samples consist of about 60–70% rhombohedral phase and are comparable regarding the phase content. The data are given in Table 3.

Rietveld refinements for sample 4 were not successful. No better goodness of fit than 2.6 was achieved (data not given). The reason for this may be a not-identified additional phase (Fig. 3b). However, a qualitative evaluation of the diffraction patterns gives strong hints for dominance of the rhombohedral phase (Fig. 3a). The lattice constants given in Table 4 are within the expected range. The data for the tetragonal phase are in correspondence

Table 3
Phase content of the fibres determined via Rietveld refinement assuming coexistence of rhombohedral and tetragonal phase. The samples were sintered at 900 °C. The doping with manganese is noted after sample number. GOF, goodness of fit; Rwp, weighted profile *R*-value; and Rp, profile *R*-value are parameters indicating the agreement between fit and measurements. The fit is the better the nearer GOF is to 1 and the smaller is Rwp and Rp, respectively.

Sample (mol% Mn)	Phase content (%)		Rwp	Rp	GOF
	Rhombohedral	Tetragonal			
1 (1.1)	63 ± 5	37 ± 5	8.92	6.79	1.29
2 (1.1)	62 ± 5	38 ± 5	11.14	8.4	1.57
3 (0.75)	67 ± 5	33 ± 5	9.03	6.83	1.43

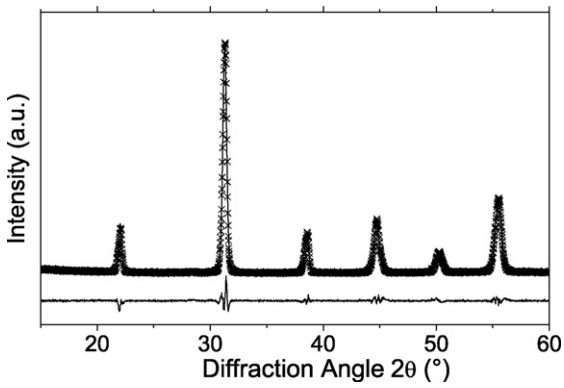

Fig. 2. Refinement results for pulverised fibres from batch 1 (sintered at 900 °C).

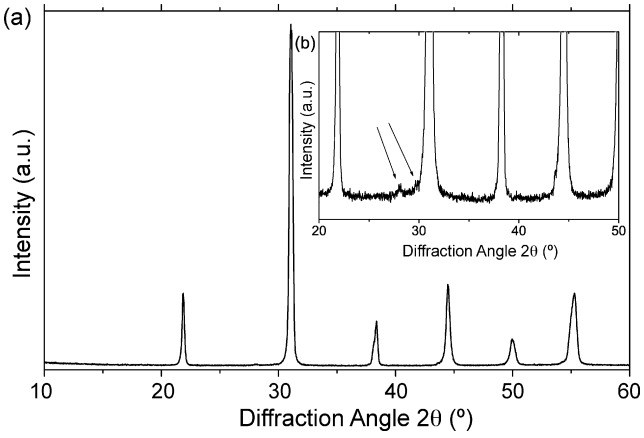

Fig. 3. (a) Powder diffraction pattern of fibres from batch 4 (sintered at 1200 °C). The detail (b) shows the reflections of a not identified additional phase. These are marked with arrows.

with the observed compression of the unit cell in *c*-direction in the vicinity of the morphotropic phase boundary.[9] Additionally, the unit cell can be compressed because of small grain sizes.[10,11]

The morphotropic phase boundary (MPB) of Nd- and Mn-codoped PZT lies around a Zr/Ti ratio of 53/47.[12] The phase composition of the sintered fibres was expected to be at the morphotropic phase boundary. The calculations revealed a relatively high content of rhombohedral phase. This result is in correspondence with the observed shift of the morphotropic phase boundary for small grain size PZT ceramics.[11] The rhombohedral phase is stabilised over the tetragonal phase. The result is a shift of the phase boundary towards higher titanium contents. However, as the *R*-values for refinement as phase mixtures of cubic and tetragonal phase are not significantly higher, it cannot be excluded that even the cubic high temperature phase is sta-

Table 4
Lattice parameters determined via Rietveld refinement. The samples were sintered at 900 °C. The doping with manganese is noted.

Sample (mol% Mn)	Rhombohedral phase		Tetragonal phase	
	a (Å)	*α* (°)	*a* (Å)	*c* (Å)
1 (1.1)	4.079	89.744	4.052	4.104
2 (1.1)	4.075	89.756	4.050	4.100
3 (0.75)	4.081	89.743	4.052	4.114

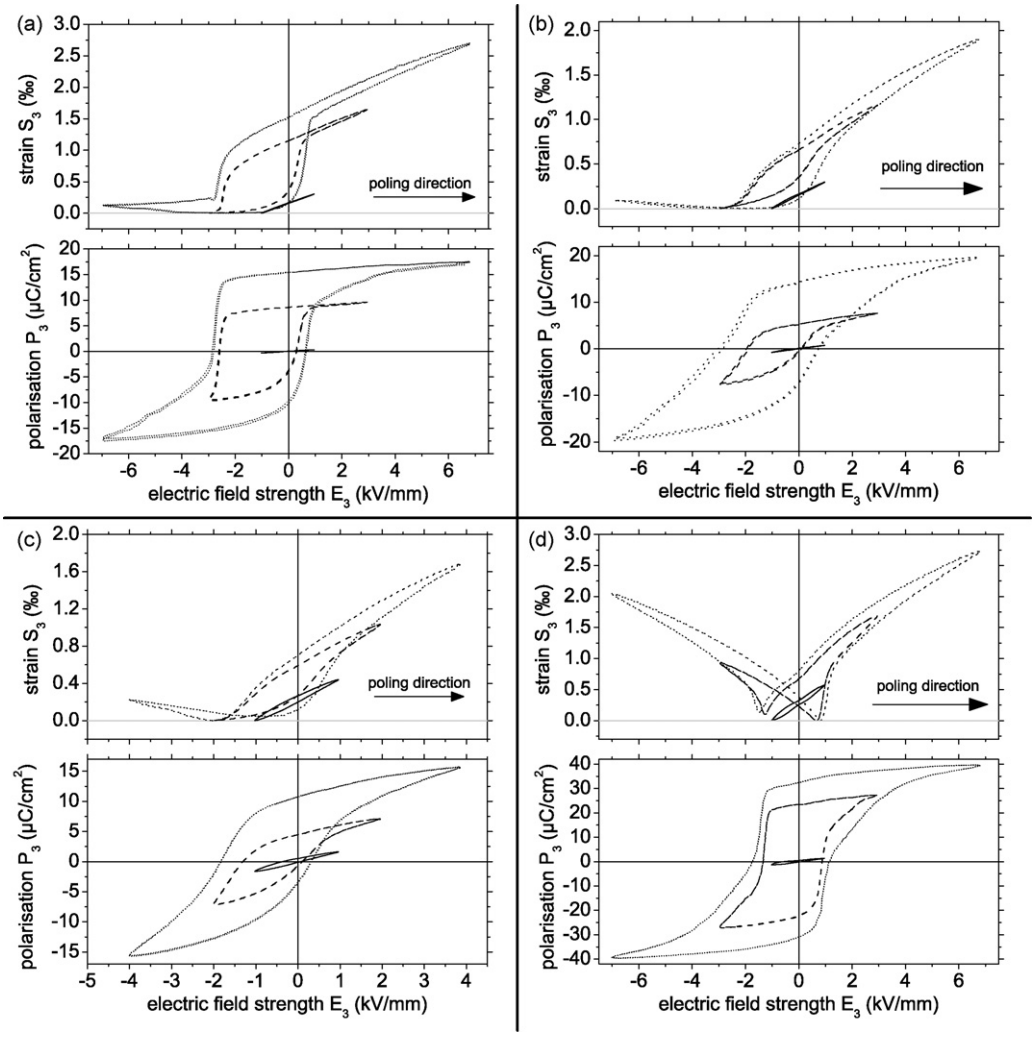

Fig. 4. Bipolar strain and polarisation hysteresis of poled samples from (a) batch 1, (b) batch 2, (c) batch 3, and (d) batch 4. The grain size increases from batch 1 to batch 4. Batch 4 was sinterd at 1200 °C, the other batches at 900 °C.

bilised to a certain degree in the sintered samples. It has to be noted that in general, Rietveld refinement of diffraction patterns of PZT ceramics in the coexistence region are affected by high uncertainty. Because of the similarity of the diffraction patterns of the two phases, strong parameter correlations occur.

4.4. Strain and polarisation hysteresis

In poled samples of batch 4 the strain hysteresis forms the well-known butterfly loops at sufficient amplitudes of electric field strengths over 1 kV/mm (Fig. 4d). Because of the previous poling process, the curves are shifted with respect to the electric field. That is, for field amplitudes of 7 kV/mm the strain switches at 0.8 kV/mm in the direction of poling and at −1.5 kV/mm in the opposite direction. Moreover, the maximum strain in poling direction (2.7‰) is larger than the one reached in the opposite direction (2.0‰). Similarly, the hysteresis of polarisation is shifted with respect to the electric field.

A similar behaviour of strain and polarisation can be observed for different batches of Nd–Mn-doped PZT with 1.5 mol% Mn and averaged grain sizes ranging from $1.5 \pm 0.6\,\mu m$ (grain size/fibre diameter = 4.1%) to $26 \pm 18\,\mu m$ (grain size/fibre diameter = 71%). These batches will be not discussed in more detail, because they class in the expected behaviour regardless of their grain size.

The strain hysteresis of samples 1 differs clearly from the butterfly loop (Fig. 4a). It is strongly asymmetric shaped with respect to the direction of the electric field. During the half period with voltage in the direction of the poling voltage, the strain hysteresis exhibits a narrow linear shape. But in the opposite direction only an inflation of the curves occurs and the strain switching is suppressed. This is clarified by the comparison of the strains reached at field amplitudes of 7 kV/mm. In poling direction the maximum strain is 2.7‰ whereas in inverted direction at −7 kV/mm it is only 0.1‰. Remarkably, for decreasing fields lower than zero the strain nearly does not change. The polarisation of these samples does not show such strong asymmetry in shape exceeding the shift of the curve due to poling. Nevertheless, the branch in poling direction is sharpened.

In order to verify the results, fibres with the same composition and sintering regime are produced (batch 2). After poling of these composites, they show a qualitatively similar behaviour

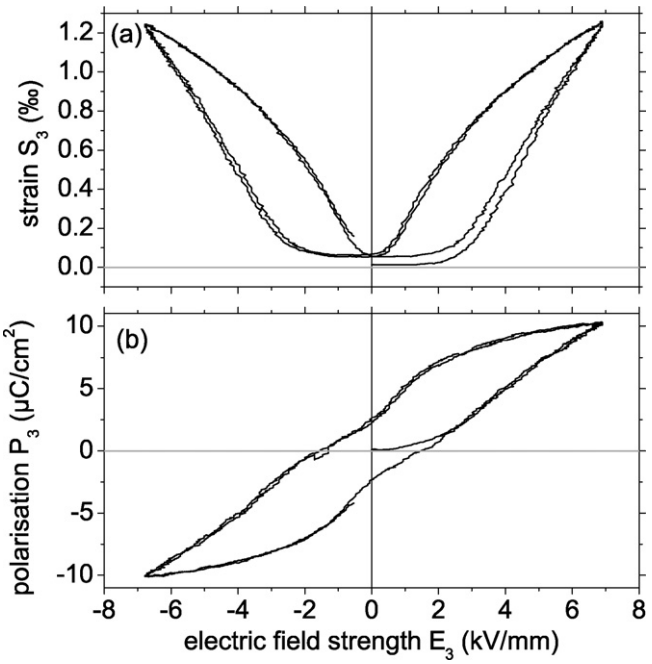

Fig. 5. Virgin loops of strain (a) and polarisation (b) of a sample frome batch 1 (sintered at 900 °C).

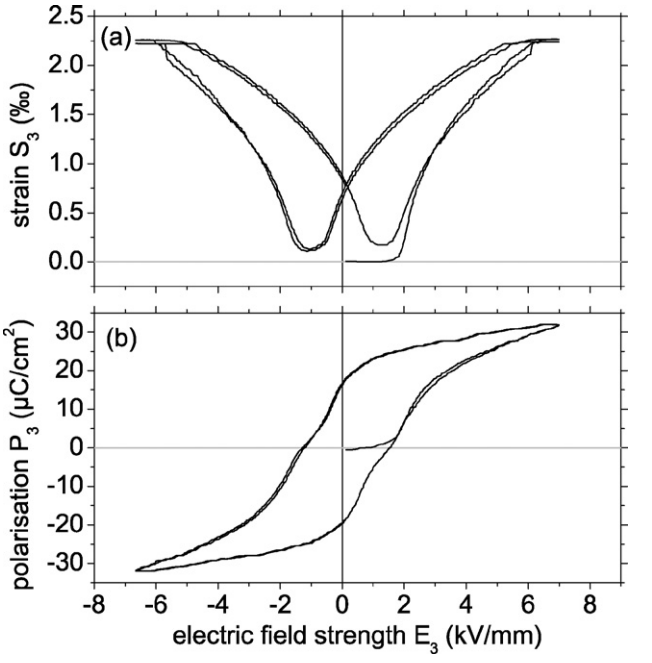

Fig. 6. Virgin loops of strain (a) and polarisation (b) of a sample from batch 4 (sintered at 1200 °C).

in strain (Fig. 4b) and polarisation compared to batch 1. The weaker inflation of the curves is noticeable. Nevertheless, the typical asymmetry of the strain curve (linear in poling direction, no decrease of strain for antiparallel to it) persists.

The observations on poled samples of batch 3 (with reduced Mn content) are different from the former observations on batches 1 and 2. Even though the shape of the strain loop (Fig. 4c) is again asymmetric with regard to poling direction in opposite direction to poling field a strain switching can be observed. A closer look at the results of batch 2 (Fig. 4b) reveals an indication for beginning of strain switching.

On samples of batch 1 virgin loops were also measured. The strain hysteresis for batch 1 (Fig. 5a) between ±2 kV/mm is flat and the initial branch is outside. The remanent strain is 0.04‰.

The virgin loop of polarisation (Fig. 5b) is constricted around the flat range of the strain hysteresis. From this curve, a coercive field strength of 1.5 kV/mm can be determined. The initial branch up to this value has a small slope and fades to saturated hysteresis loop clearly before the maximum polarisation is reached.

As previously described, the poling process is not only a long lasting electrical load but also a temperature load. In order to test its influence on the virgin strain loops one sample was tempered in the described poling procedure but without voltage. Afterwards its virgin loop does not change qualitatively. Hence, the temperature regime during poling does not influence the forming of hysteresis loops.

Contrary to the former results, the virgin loops of the high temperature sintered samples of batch 4 show the typical behaviour as it can be expected for ferroelectrics (Fig. 6). The virgin loop of strain (Fig. 6a) exhibits the butterfly shape. The strain is obviously switched. The remanent strain is about 0.7‰. The electric field strength for the strain minima is 1.2 kV/mm. That corresponds to the coercive field strength measured from the virgin loop of polarisation (Fig. 6b). Until the coercive field is reached, the virgin loop of strain is flat. The corresponding range of the polarisation loop shows a small slope and reaches subsequent the saturated polarisation loop. This region resembles in appearance the comparable one of batch 1.

5. Discussion of the asymmetric strain loops

In the following section the unexpected asymmetric strain behaviour of the samples and possible explanations shall be discussed.

The question arises, whether the observed asymmetric strain loops of batches 1–3 could be generated by buckling of the fibres. According to Euler's buckling theory the buckling stress of free fibres rises with the squared fibre diameter. The fibre diameter decreases from batch 1 to batch 4. The according buckling stress for batch 4 is nearly 20% of the one needed for batch 1. Because strain loops of batch 4 give no reason considering buckling effects they appear even more implausible for the other batches.

Due to poling, a remanent strain is induced in the ceramic fibres. If the fibre content is too small, the clamping by the polymer matrix can cause a depolarisation. The calculation for an mechanical similar composite in Ref. [13] was adapted. Considering the approximately half Young's modulus of the polymer here and neglecting differences of the ferroelastic behaviour of the fibres it can be concluded that the maximal fibre content causing a depolarisation of the samples is smaller than 6.1%. The fibre content of the samples discussed in this paper is more than five times higher. Moreover, the samples with the smallest fibre content (batch 4) exhibit the most expected strain–field behaviour.

The calculations in Ref. [13] show that the lateral stresses can be neglected in comparison with the longitudinal stresses in poling direction. So the stresses can be guessed as uniaxial. According to results on PZT-5H[14] for uniaxial mechanical prestress, only a decrease of strain-amplitude can then be expected even for poled samples. However, the butterfly shape of the strain hysteresis retains in that case and is only shifted. Consequently, the anomalous shape of the strain loops is considered as not caused by poling forced internal stress. As result, the origin of the asymmetry can be strongly assumed to be a pure feature of the ceramics. For this reason the discussion is now forced on the properties of the used PZT fibres.

Due to an internal offset of electric field or polarisation, the hysteresis curves may be shifted and deformed. An internal polarisation offset would also cause an asymmetric strain hysteresis.[15] The symmetric virgin loops indicate that there are no internal electric fields or polarisations due to the fabrication of the samples. Evidently, poling provides an imprint of asymmetry. Nevertheless the observed strain loops strongly exceed a pure shrinkage of branches asymmetrically with respect to the polarity of the applied voltage. Therefore, they cannot be explained by internal offsets of field or polarisation. In fact a reason in domain configuration or phase interaction has to be assumed.

The forming of the asymmetric strain loops (Fig. 4a–d) increases from batch 4 (only a shift (d)), batch 3 (small strain switching (c)), batch 2 (hardly any strain switching (b)) to batch 1 (no strain switching (a)). This order correlates with the grain sizes themselves and with the ratio between grain sizes and fibre diameter (Table 1). The smaller this ratio, the clearer is the asymmetry of strain loops.

The grains at the fibre surface can be regarded as a less strained material than the subsurface (bulk) material. Therefore, the higher the specific surface (the thinner the fibre) the lower should be the content of strained material. In fact, the fibre diameters decrease from batch 1 to batch 4. That means, that strain due to the surface of the fibres does not determine the observed special strain loops.

Due to formation of domains the mechanical stress is weakened in coarse grained ceramics. By contrast, in small grains this process could be partially blocked. Therefore, the domain wall motion is constrained. From this follows a reduction of switchable polarisation and strain. On the other hand, the internal mechanical stress distorts the lattice in the grains and therefore may modify the phase content of the ceramics.

In PZT the lattice distortion of the tetragonal phase is higher than for rhombohedral phase.[16] In addition, the tetragonal phase in PZT is mechanical stiffer than the rhombohedral phase.[17] Consequently, the reorientation of domains should be blocked less in the rhombohedral phase. The analysis of phase content (Table 3) and the higher Zr/Ti ratio of batch 4 compared with batch 1 (Table 2) suggests the possibility that batches 3 and 4 possess a higher content of rhombohedral phase than the other batches. The observations of strain switching on batches 3 and 4 are not contrary to this trend. However, the phase content was measured on pulverised and unpoled fibres. Because pulverisation partially destroys the mechanical interaction between the ceramic grains one specific effect of the grain size likely diminishes in the examination of phases.

The virgin strain loop of samples from batch 1 suggests a relaxor behaviour. Dielectric spectroscopic measurements done at Jožef Stefan Institute Ljubljana (Slovenia) are contrary to this. Within the frequency range of 1 Hz to 100 kHz no significant change of the relation between dielectric coefficients and temperature (ranging between −70 °C and 70 °C) was observed. Poled samples also do not exhibit relaxor properties.[18] In addition to this, the samples from batch 1 are clearly not antiferroelectric, as their polarisation loop shows. This can be expected, because only for lead zirconate[19] or Zr-rich PZT compositions[20] antiferroelectricity is reported.

However, the double branched virgin loop of strain of batch 1 (Fig. 5) indicates a stabilisation of the unpoled state in the ceramics. It could be generated by mechanical clamping due to the small grain size.

6. Conclusions

On poled fibre composites an asymmetry of the strain–field curves could be observed. The results not only proofs reproducibility of the effect but also give strong hints to a sensitive material dependence that is believed to be attributed solely to the ceramic fibres. The asymmetry of the strain loops is clearly correlated with the grain size and the doping with manganese. The small dimensions of grains encourage the assumption of intergranular stress. Whether these stresses influence the phase content cannot be surely decided.

Apparently the strain switching is blocked. The stabilisation of the domain structure is likely reinforced by the doping with manganese. The poling process provides an imprint of asymmetry that results in a blocking of strain switching in some regions of the ceramics. The non-90°-processes seem to be partially suppressed in reverse poling direction, at least for periodic electric loads. Only a long lasting electric field enables switching of the regions. On the other side, the polarisation switching 180°-processes are possible.

Acknowledgements

We are indebted to Dr. J. Berndt-Gerdes (Insitute for Mineralogy, University of Münster) for Microprobe analysis and Dr. V. Bobnar (Jožef Stefan institute, Ljubljana, Slovenia) for dielectric spectroscopy of some samples. Our special thanks go to Dr. K. Lubitz and Prof. Dr. G. Schmidt for the discussions.

The authors gratefully acknowledge the support by the German Ministry of Education and Research (promotional reference: 03X4001) within the WING-Programme.

References

1. Setter, N., ed., *Piezoelectric materials in devices*. Ceramics Laboratory, EPFL Swiss Federal Institute of Technology, Lausanne, 2002.
2. Jaffe, B., Cook, W. R. and Jaffe, H., Piezoelectric ceramics. In *Non-metallic solids*, *vol. 3*. Academic Press, London/New York, 1971.
3. Kungl, H., Fett, T., Wagner, S. and Hoffmann, M. J., Nonlinearity of strain and strain hysteresis in morphotropic LaSr-doped lead zirconate titanate

under unipolar cycling with high electric fields. *J. Appl. Phys.*, 2007, **101**(4), 044101.
4. Lupascu, D. C. and Verdier, C., Fatigue anisotropy in lead–zirconate–titanate. *J. Eur. Ceram. Soc.*, 2004, **24**(6), 1663–1667.
5. Sorge, G., Hauke, T. and Klee, M., Electromechanical properties of thin ferroelectric $Pb(Zr_{0.53}Ti_{0.47})O_3$-layers. *Ferroelectrics*, 1995, **163**, 77–88.
6. Steinhausen, R., Hauke, T., Beige, H., Watzka, W., Lange, U., Sporn, D., Gebhardt, S. and Schönecker, A., Properties of fine scale piezoelectric PZT fibers with different Zr content. *J. Eur. Ceram. Soc.*, 2001, **21**(10–11), 1459–1462.
7. Holman, R. L. and Fulrath, R. M., Intrinsic nonstoichiometry in lead zirconate–lead titanate system determined by Knudsen effusion. *J. Appl. Phys.*, 1973, **44**(12), 5227–5236.
8. Chandrasekharaiah, M. S., Volatility of refractory inorganic compounds. In *The characterization of high-temperature vapors*, ed. J. L. Margrave. John Wiley & Sons, New York, 1967, pp. 495–507.
9. Wersing, W., Rossner, W., Eckstein, G. and Tomandl, G., Morphotropic phase boundary in PZT ceramics prepared by spray-drying of salt solutions and by the mixed oxide method. *Silic. Ind.*, 1985, **50**(3–4), 41–46.
10. Randall, C. A., Kim, N., Kucera, J.-P., Cao, W. and Shrout, T. R., Intrinsic and extrinsic size effects in fine-grained morphotropic-phase-boundary lead zirconate titanate ceramics. *J. Am. Ceram. Soc.*, 1998, **81**(3), 677–688.
11. Helbig, U., Size effect in low grain size neodymium doped PZT ceramics. *J. Eur. Ceram. Soc.*, 2007, **27**(7), 2567–2576.
12. Bödinger, H., Lubitz, K. and Schuh, C., Piezoceramic composition, piezoceramic body comprising said composition and a method for producing said composition and said body. Patent specification WO/2003/101946.
13. Hauke, T., Steinhausen, R., Seifert, W., Beige, H. and Kamlah, M., Modeling of poling behavior of ferroelectric 1–3 composites. *J. Appl. Phys.*, 2001, **89**(9), 5040–5047.
14. Chaplya, P. M. and Carman, G. P., Dielectric and piezoelectric response of lead zirconatelead titanate at high electric and mechanical loads in terms of non-180° domain wall motion. *J. Appl. Phys.*, 2001, **90**(10), 5278–5286.
15. Lupascu, D. and Rödel, J., Fatigue in bulk lead zirconate titanate actuator materials. *Adv. Eng. Mater.*, 2005, **7**(10), 882–898.
16. Hoffmann, M. J., Hammer, M., Endriss, A. and Lupascu, D. C., Correlation between microstructure, strain behavior, and acoustic emission of soft PZT ceramics. *Acta Mater.*, 2001, **49**(7), 1301–1310.
17. Schäufele, A. B. and Härdtl, K. H., Ferroelastic properties of lead zirconate titanate ceramics. *J. Am. Ceram. Soc.*, 1996, **79**(10), 2637–2640.
18. Bobnar, V., Private communication, 2007.
19. Shirane, G., Sawaguchi, E. and Takagi, Y., Dielectric properties of lead zirconate. *Phys. Rev.*, 1951, **84**(3), 476–481.
20. Davis, M., Damjanovic, D. and Setter, N., Electric-field-, temperature-, and stress-induced phase transitions in relaxor ferroelectric single crystals. *Phys. Rev. B*, 2006, **73**(1), 014115.